ADVANCED MATERIALS
www.advmat.de

Topological Engineering of Pt-Group-Metal-Based Chiral Crystals toward High-Efficiency Hydrogen Evolution Catalysts

Qun Yang, Guowei Li, Kaustuv Manna, Fengren Fan, Claudia Felser,* and Yan Sun**

It has been demonstrated that topological nontrivial surface states can favor heterogeneous catalysis processes such as the hydrogen evolution reaction (HER), but a further decrease in mass loading and an increase in activity are still highly challenging. The observation of massless chiral fermions associated with large topological charge and long Fermi arc (FA) surface states inspires the investigation of their relationship with the charge transfer and adsorption process in the HER. In this study, it is found that the HER efficiency of Pt-group metals can be boosted significantly by introducing topological order. A giant nontrivial topological energy window and a long topological surface FA are expected at the surface when forming chiral crystals in the space group of $P2_13$ (#198). This makes the nontrivial topological features resistant to a large change in the applied overpotential. As HER catalysts, PtAl and PtGa chiral crystals show turnover frequencies as high as 5.6 and 17.1 s^{-1} and an overpotential as low as 14 and 13.3 mV at a current density of 10 mA cm^{-2}. These crystals outperform those of commercial Pt and nanostructured catalysts. This work opens a new avenue for the development of high-efficiency catalysts with the strategy of topological engineering of excellent transitional catalytic materials.

With the increase of global energy consumption and related environmental degradation from fossil fuels, the study of new types of energy carriers has attracted tremendous attention in the last decades. Hydrogen is an ideal renewable future energy carrier because of its high-energy density without carbon emission.[1–3] The development of highly efficient stable electrocatalysts for hydrogen evolution reaction (HER) has been one of the most important research topics for the generation and utilization of hydrogen.[4–8] Pt-group metals, especially Pt, are ideal catalysts for various heterogeneous catalysis such as electrochemical HER. These metals are located near the top of the HER volcano plot with favorable Gibbs-free energy for hydrogen adsorption, thus exhibiting the state-of-the-art high efficiency.[9–12] Recent studies have confirmed that the performance of these metals can be optimized by employing strategies such as nanostructuring, defect introduction, or use of single-atom catalysts.[6,13]

The observation of the topological order in materials provides an extra reasonable solution for the design of high-efficiency catalysts. To date, the introduction of the topological order is theoretically and experimentally demonstrated to be effective in tailoring adsorption and catalytic processes in the fields of hydrogen evolution, oxygen evolution, and CO oxidation, etc.[14–20] The situation looks perfect! Unfortunately, there are still no candidates that can outperform the state-of-the-art pure noble metals. So far, for the topological catalysts that have been studied, it seems that the topological band structure can improve the catalytic properties, but only to a finite level. Based on conventional knowledge, the d-band plays an important role in determining catalytic efficiency,[21] whereas most of the topological materials are constructed by the s- and p-orbitals.[22,23] A good combination of d-band and topological band structures has not been investigated in topological catalysts yet. This phenomenon inspired us to combine the topological surface states and traditional high-efficiency parental catalysts, especially Pt.

Herein, we report several Pt-group-metal-based chiral topological catalysts that show remarkably high HER activities, with an extremely low overpotential of 14 and 13.3 mV at a current density of 10 mA cm^{-2} for PtAl and PtGa crystals, respectively, along with record-high turnover frequencies (TOFs). We demonstrate that the topologically protected features persist under large chemical potential change induced by H adsorption and play an important role in surface catalytic reactions. Thus, the chiral crystals PtGa and PtAl can deliver an exceptionally high current density of 600 mA cm^{-2} at an ultralow overpotential of 113 and 151 mV, respectively. Because of the advantages of high activity, stability, and low noble metal loading, the chiral compounds could be an alternative to pure commercial Pt for large-scale hydrogen production.

The proposed strategy is shown in **Figure 1**A. Although Pt itself contains a Z_2 topological index, the topological band structure is far away from the Fermi level, and it is constructed by s and p orbitals, but not d orbitals. The bands around the Fermi level are mainly dominated by the 5-d orbitals,[24] which

Q. Yang, Dr. G. Li, Dr. K. Manna, Dr. F. Fan, Prof. C. Felser, Dr. Y. Sun
Max Planck Institute for Chemical Physics of Solids
Nöthnitzer Str. 40, Dresden 01187, Germany
E-mail: Guowei.Li@cpfs.mpg.de; Claudia.Felser@cpfs.mpg.de; Yan.Sun@cpfs.mpg.de

Prof. C. Felser
Center for Nanoscale Systems
Faculty of Arts and Sciences
Harvard University
Oxford Str. 11, LISE 308, Cambridge, MA 02138, USA

The ORCID identification number(s) for the author(s) of this article can be found under https://doi.org/10.1002/adma.201908518.

DOI: 10.1002/adma.201908518

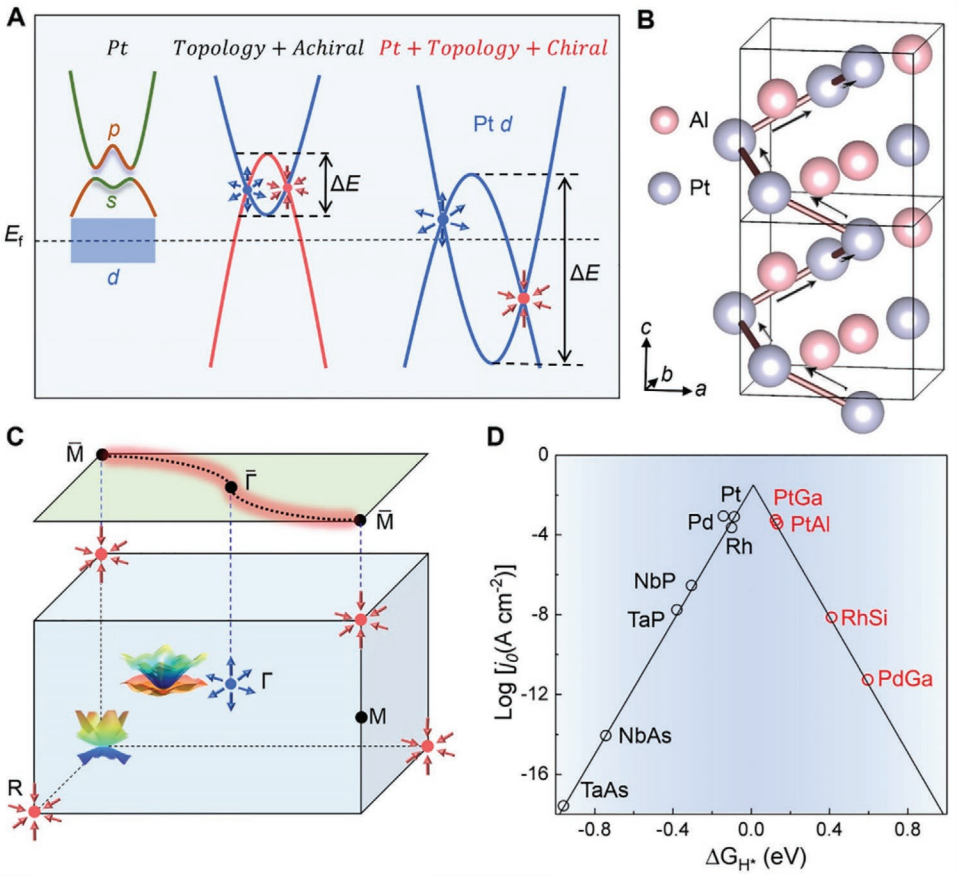

Figure 1. Chiral crystal structure protected multifold Fermions and corresponding catalytic properties. A) Illustration of the band inversion mechanism and topologically nontrivial energy window in pure Pt,[24] nonchiral topological semimetals, and chiral B20 compounds. B) Crystal structure of PtAl with space groups $P2_13$ (No. 198). The c_2 screw rotation symmetry along [001] direction is highlighted by arrows. C) Bulk Brillouin zone (BZ) and its projection to the (001) surface. A doubly degenerated Weyl and fourfold degenerated Rarita–Schwinger Weyl points locate at Γ points. A sixfold degenerated point locates at R points. The topological charges at Γ and R points are +4 and −4, respectively. The Fermi arcs connect high symmetry points of $\overline{\Gamma}$ and $\overline{M}$. D) HER volcano plot of PtAl, PtGa, RhSi, PdGa, and the related metal catalysts (the experimental data of Rh, Pd, and Pt).[42] The topological Weyl semimetals NbP, TaP, NbAs, and TaAs (the calculated data)[14] are also presented for comparison.

are also believed to be the cause of high Pt catalytic efficiency. In other catalysts with topological order, such as Weyl semimetal and topological insulators, the nontrivial energy window is very small, and the enhancement of HER performance from topological band structures is strongly limited. On the other hand, if one can have a Pt-d orbital derived topological band structure along with a large nontrivial energy window (see the right panel of Figure 1A), significant improvement in the efficiency is expected for Pt-based catalysts.

Thanks to the development of topological materials, a new type of topological semimetals of multifold fermions were theoretically predicted and experimentally verified in a class of chiral crystals.[25–31] Owing to the chiral crystal symmetry, the band structures of this type of materials present as multifold degenerated points with a large topological charge of Chern number 4 (Figure 1B,C). Unlike topological insulators and Weyl semimetals, the sources of topological charges in this type of materials locate at different high symmetry time-reversal invariant momenta, which guarantee giant nontrivial energy windows and long surface Fermi arcs, as presented in Figure 1A,C. This type of topological materials contains Pt-related compounds, such as PtAl, PtMg, and PtGa, which provide the ideal platform to topologically enhance the catalytic efficiency based on the traditional good catalyst of Pt.

Based on this motivation, we directly calculated the Gibbs-free energies of the H adsorption $|\Delta G_{H^*}|$ for two experimentally verified Pt-contained multifold Fermi topological semimetals, PtAl, and PtGa (Figure 1D). For comparison, some typical catalysts from transition metals, topological materials, and other two Pt-free chiral topological semimetals are also shown in the same volcano plot. From the calculated $|\Delta G_{H^*}|$ (0.131 eV for PtGa and 0.132 eV for PtAl), one can easily see that the predicted exchange current density in PtGa and PtAl is much higher than those of the other topological materials and as good as that of Pt.

To understand the origin of the excellent HER activity in Pt-based chiral crystal topological semimetals, we investigated their surface states and the influence on the hydrogen adsorption. According to previous experimental reports, the easy-cleaving plane is along the (001) direction. Due to the presence of a twofold screw axis along z, there is only one type of surface termination,[25,27–30] as schematically shown in **Figure 2**A.

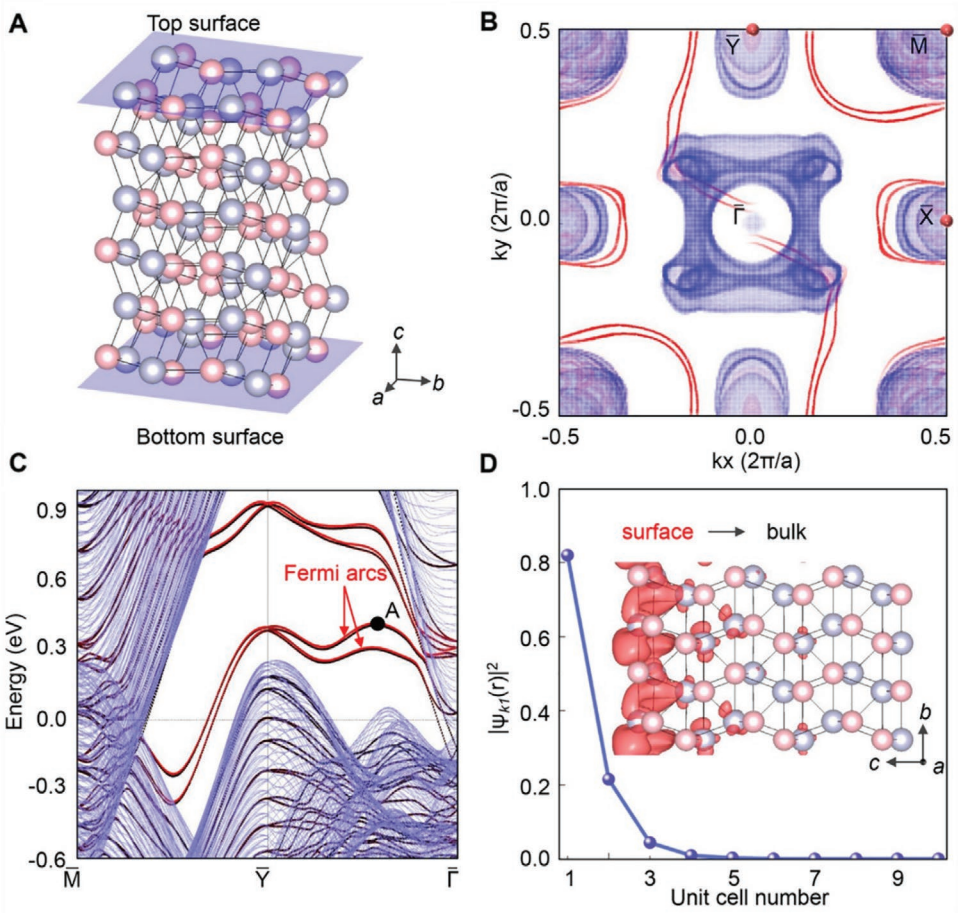

Figure 2. (001) surface electronic structures of pristine PtAl. A) Schematic of PtAl (001) slab model, herein, the thickness of three unit cells is displayed, while the slab with ten unit cells thickness was used in calculations. B) Surface FS of PtAl (001) with energy at the Fermi level. C) Surface energy dispersion. The surface states from the top surface are highlighted by the red line. The bulk projected states are shown in blue as the background. D) Surface states contribution as a function of the distance away from the top surface. The wave function at the sample point A in (C) is applied. The inset is real space partial charge density distributions of the Fermi arc at the sample point A with an isosurface value of 0.0015 e Å^{-3}.

Taking PtAl as an example, the surface states are analyzed in a slab model with a thickness of 10 unit cells separated by a vacuum space of 15 Å. As presented in Figure 2B,C, with the topological charge of Chern number ±4 at Γ and R points in the bulk band structure, two Fermi-arc-related surface states connect to the projected $\overline{\Gamma}$ and $\overline{M}$ points along the high symmetry lines. Owing to the large nontrivial energy window, the Fermi-arc-related bands can extend from ≈–0.3 to ≈0.3 eV along $\overline{M}$–$\overline{Y}$–$\overline{\Gamma}$ high symmetry path and the surface states are dominated by the Fermi arcs in this energy window. Hence, the surface adsorption and reaction processes should be closely related to the topological Fermi arcs.

Interestingly, it is found that the Fermi arcs are mainly contributed from the surface Pt-d orbitals (see Figure S5, Supporting Information), which provides an excellent combination of topological surface states and element Pt. Because of the large inverted band gap, the Pt-d orbital dominated Fermi arcs are localized on the surface with a thickness of two unit cells. The contribution ratio of an arbitrarily selected point A (see Figure 2C) from the Fermi arc is ≈80% for the top one unit cell, and it dramatically decreases to ≈0 for the third unit cell away from the surface (Figure 2D). Therefore, the chemical reaction of the catalytic process mainly occurs with Fermi arcs from the top four Pt atom layers. In addition, the large proportion of d orbitals in the surface states, rather than the s or p orbitals in the other topological catalysts,[13,16,17] indicating a favorable interaction between the adsorbate and the catalysts surface based on the d-band theory.[15]

Indeed, this is confirmed by analyzing the H adsorption on PtAl crystal surface. After the relaxation of top-three unit cells of PtAl and the adsorbed H, it is found that the H prefers to stay above atom Pt (**Figure 3**A) with negative adsorption energy (E_a) of –0.098 eV, representing a relatively weak adsorption strength, which is beneficial for the desorption process in HER, thereby leading to a low Tafel slope as observed in the experimental results. Moreover, a similar analysis also works for the other three chiral crystals, and the corresponding adsorption energies were calculated to be –0.099, 0.166, and 0.352 eV for PtGa, RhSi, and PdGa, respectively.

After H adsorption, the topological Fermi arcs change dramatically in both momentum and energy spaces, as indicated in Figure 3B,C. Meanwhile, as plotted in Figure 3D,E, the charge depletion happens on the surface Pt atoms with d orbital characteristics, while the charge accumulation occurs around

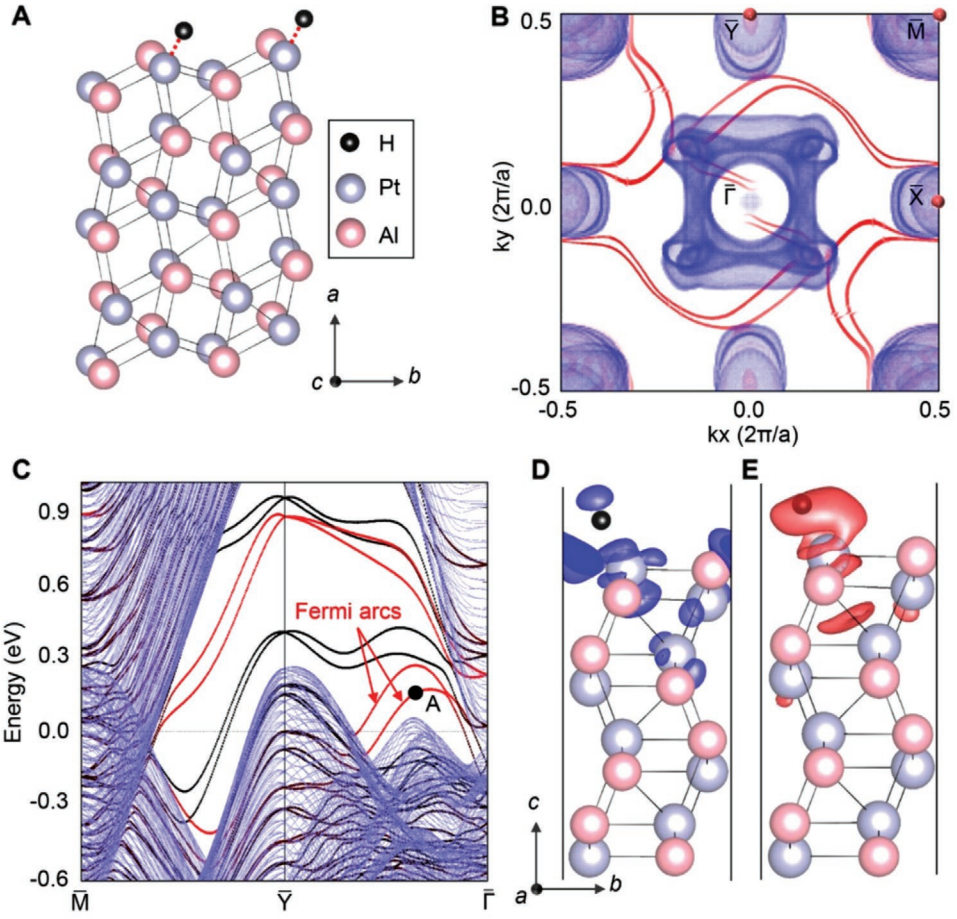

Figure 3. Change of PtAl (001) surface states after H adsorption. A) The most energetic favorable site for H adsorption. B) Surface FS of PtAl (001)-H with chemical potential at charge neutral point. C) Surface energy dispersion after H-adsorption. D,E) The charge density difference plot of PtAl (001)-H; the blue and red areas in (D,E) represent the electron depletion and accumulation, respectively. The isosurface values are all set to 0.0015 e Å^{-3}.

the adsorbed H with s orbital shape. The H 1s bands disperse in the deep energy region below the Fermi level (Figure S7, Supporting Information), which further illustrates the charge transfer to H. After the H adsorption, although the detailed shape of the Fermi arcs considerably changes, their topological features of chirality, number of Fermi arcs, and connection do not change because of the robust topological charges. Similar changes are also observed in the other three chiral counterparts as shown in Figure S9 (Supporting Information). This suggests the high-stability of the surface states after H adsorption. Moreover, the partial unoccupied topological Fermi arcs shift down by accepting the part of electrons provided by the trivial surface states, as indicated in Figure 3C and Figure S10 (Supporting Information). Therefore, the topological Fermi arcs from d-orbitals of the transition elements weaken the binding strength toward H adsorption and play a decisive role in imparting excellent HER catalytic efficiency (the detailed analysis is given in the Supporting Information).

Although PtGa and PtAl are expected to be good catalysts that comparable to Pt, the DFT calculation has its own accuracy limit.[32–34] Moreover, the calculated $|\Delta G_{H^*}|$ is very close to the peak in the volcano plot. Thus, it is a big challenge to quantitatively compare the efficiency of Pt catalyst and these two Pt-based topological compounds, especially the intrinsic efficiency. To verify our hypothesis, high-quality bulk single crystals with a well-defined surface are needed.

High-quality chiral crystals including PtAl, PtGa, PdGa, and RhSi were synthesized according to our previous studies.[26,35,36] Briefly, polycrystalline ingots with a stoichiometric amount of high purity Pt-group metals and X element (X = Al, Si, or Ga) were obtained by arc melting. Bulk single crystals were obtained by the flux technique with different heating procedures (details are provided in Supporting Information). Crystals with diameters from several millimeters to centimeters can be collected after cooling to room temperature. The presence of the sharp diffraction spots in the corresponding Laue diffraction pattern suggests the high quality of the bulk single crystals (Figure S12, Supporting Information). The high quality of the chiral crystals were further proved by the well-defined powder X-ray diffraction (XRD) patterns as displayed in Figure S13 (Supporting Information). These crystals adopt the cubic structure and are oriented along the [001] direction with lattice parameters of a = 4.863 Å, a = 4.911 Å, a = 4.896 Å, and a = 4.686 Å for PtAl, PtGa, PdGa, and RhSi, respectively.

To evaluate the HER catalytic activities, the chiral crystals were attached to a Ti wire and served as both the electrodes and

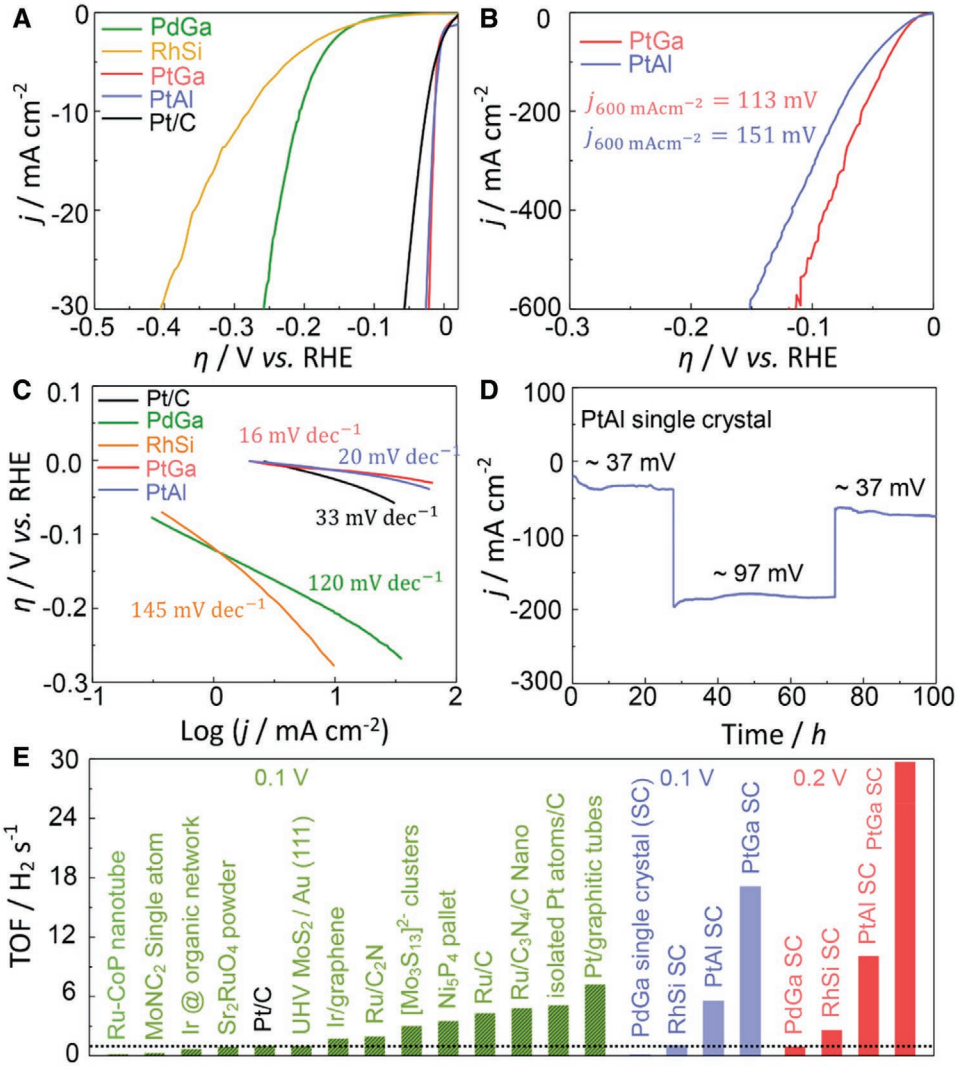

Figure 4. HER performance of the chiral crystal catalysts. A) Polarization curves of the chiral crystal catalysts: PdGa, RhSi, PtAl, PtGa, and 20% Pt/C catalysts. B) Polarization curves of PtAl and PtGa at higher applied overpotentials. C) Tafel plots of the chiral crystal catalysts: PdGa, RhSi, PtAl, PtGa, and 20% Pt/C catalysts. D) Stability test of the PtAl single-crystal catalyst at different overpotentials for 100 h. E) Comparison of TOF values between the chiral crystal catalysts and state-of-the-art noble metal-based nanostructured electrocatalysts.

catalysts. All experiments were performed in a three-electrode electrochemical cell (Ar-purged 0.5 M H_2SO_4 (aq)). The linear-sweep voltammograms (LSVs) normalized to the projected geometric area of the crystals are shown in **Figure 4**A and compared against commercial 20% Pt/C nanostructured catalysts. The overpotential of Pt/C at a current density of 10 mA cm^{-2} is 25 mV, with an extremely low onset overpotential of ≈0 mV. In comparison, PdGa and RhSi chiral crystals require an overpotential of 207 and 280 mV to deliver the same current density. In sharp contrast, PtGa and PtAl chiral crystals can effectively catalyze HER with an extremely low overpotential of 13.3 and 14 mV at a current density of 10 mA cm^{-2}, respectively. In addition, both these chiral crystals could deliver an exceptionally high current density of 600 mA cm^{-2} with an ultralow overpotential (113 mV for PtGa, and 151 mV for PtAl), as indicated by the iR-corrected curve in Figure 4B. These results indicate that single crystals can be used as both electrode and catalysts, which favor the transfer of electrons to the active sites at the crystal surfaces.

Tafel slopes showed in Figure 4C provides additional information about the HER mechanism. Notably, the Tafel slopes for PtGa and PtAl chiral crystals are only 16 and 20 mV dec^{-1}, respectively, which are even lower than that of the Pt/C catalyst (33 mV dec^{-1}). This suggests that the rapid desorption of two hydrogen atoms is the rate-determination step on the chiral crystal surface.[5] The simultaneous change between current density and applied voltage reveals the excellent mass transport and mechanical robustness of the single crystal catalyst (Figure S14, Supporting Information). Additionally, the PtAl chiral crystal was selected for stability investigation due to its low cost. The long-term chronoamperometry (CA) testing shows no decrease in the current density during the continuous HER for up to 100 h, even at a high current density of 200 mA cm^{-2}, indicating the high HER operational stability of the chiral crystal catalyst (Figure 4D).

The intrinsic HER activity was critically evaluated by measuring the TOF of the chiral crystals, which is associated with the number of hydrogen molecules evolved per second per active site.[37] In this study, the HER activities were normalized by the electrochemical active surface area (ECSA) to provide a fair comparison of the TOF values (Figure S15, Supporting Information). The results reveal that the TOF values follow the order PtGa > PtAl > RhSi > PdGa, which is consistent with the thermodynamic parameter of Gibbs-free energy, as indicated in Figures 4E and 1D. Particularly, at a constant overpotential of 100 mV, the chiral crystals of PtGa, PtAl, and RhSi electrocatalysts deliver an extremely high TOF value of 17.1, 5.6, and 1.1 s^{-1}, respectively. The TOF value is increased to 10.1 and 29.7 s^{-1} for PtAl and PtGa electrocatalysts at an overpotential of 200 mV, respectively, setting these chiral crystals as the benchmark catalysts for HER (Figure 4E). These values are not only evidently larger than those of nanostructured electrocatalysts but also more strikingly superior to the values obtained for commercial Pt/C and some well-known noble-metal-based HER catalysts.[3,5,37–41]

Excellent new electrocatalysts were discovered by applying the proposed strategy of topological engineering of Pt-group metals. With enhancement from topological band structures based on Pt, multifold fermion chiral compounds show exceptionally high activity as HER catalysts with an extremely low overpotential and Tafel slope as well as considerably high TOF and operational stability superior to that of the commercial Pt/C catalyst, making them the benchmark for HER catalysts. Our theoretical analysis reveals that the giant Fermi arcs and nontrivial energy window in the studied topological chiral crystals are robust against H adsorption. The topologically protected surface states originating from the d orbitals of the surface transition metal atoms could weaken the interaction between H adsorption and substrate, thus intrinsically boosting the H desorption kinetics. Our work provides a new approach to design highly efficient catalysts by introducing the topological order in Pt-group metals.

Supporting Information

Supporting Information is available from the Wiley Online Library or from the author.

Acknowledgements

This work was financially supported by the European Research Council (ERC Advanced Grant No. 291472 "Idea Heusler") and ERC Advanced Grant (No. 742068)—TOPMAT.

Author Contributions

Q.Y. and G.L. contributed equally to this work. Y.S., G.-L., and C.F. supervised the project and designed the research. Q.Y. performed the theoretical calculation and analysis, G.-W.L. performed electrochemical measurements and analysis. K.M. performed material synthesis and characterizations. F.-R.F. assisted with the theoretical analysis. Q.Y., G.-W.L., and Y.S. cowrote the paper. All authors discussed the results and commented on the manuscript.

Conflict of Interest

The authors declare no conflict of interest.

Keywords

chiral crystals, electrocatalysts, hydrogen evolution, Pt-group metals, topological engineering

Received: December 30, 2019
Revised: January 22, 2020
Published online: February 20, 2020

[1] X. Wang, K. Maeda, A. Thomas, K. Takanabe, G. Xin, J. M. Carlsson, K. Domen, M. Antonietti, *Nat. Mater.* **2009**, *8*, 76.
[2] J. Turner, *Science* **2004**, *305*, 972.
[3] J. Mahmood, M. A. R. Anjum, S. H. Shin, I. Ahmad, H. J. Noh, S. J. Kim, H. Y. Jeong, J. S. Lee, J. B. Baek, *Adv. Mater.* **2018**, *30*, 1805606.
[4] R. Subbaraman, D. Tripkovic, D. Strmcnik, K. C. Chang, M. Uchimura, A. P. Paulikas, V. Stamenkovic, N. M. Markovic, *Science* **2011**, *334*, 1256.
[5] J. N. Tiwari, S. Sultan, C. W. Myung, T. Yoon, N. N. Li, M. R. Ha, A. M. Harzandi, H. J. Park, D. Y. Kim, S. S. Chandrasekaran, W. G. Lee, V. Vij, H. J. Kang, T. J. Shin, H. S. Shin, G. Lee, Z. Lee, K. S. Kim, *Nat. Energy* **2018**, *3*, 773.
[6] M. F. Li, K. N. Duanmu, C. Z. Wan, T. Cheng, L. Zhang, S. Dai, W. X. Chen, Z. P. Zhao, P. Li, H. L. Fei, Y. M. Zhu, R. Yu, J. Luo, K. T. Zang, Z. Y. Lin, M. N. Ding, J. Huang, H. T. Sun, J. H. Guo, X. Q. Pan, W. A. Goddard, P. Sautet, Y. Huang, X. F. Duan, *Nat. Catal.* **2019**, *2*, 495.
[7] J. Zhang, K. Sasaki, E. Sutter, R. Adzic, *Science* **2007**, *315*, 220.
[8] G. Chen, T. Wang, J. Zhang, P. Liu, H. Sun, X. Zhuang, M. Chen, X. Feng, *Adv. Mater.* **2018**, *30*, 1706279.
[9] Z. W. Seh, J. Kibsgaard, C. F. Dickens, I. Chorkendorff, J. K. Norskov, T. F. Jaramillo, *Science* **2017**, *355*, eaad4998.
[10] J. Greeley, T. F. Jaramillo, J. Bonde, I. Chorkendorff, J. K. Nørskov, *Nat. Mater.* **2006**, *5*, 909.
[11] Z. Geng, X. Jin, R. Wang, X. Chen, Q. Guo, Z. Ma, D. Dai, H. Fan, X. Yang, *J. Phys. Chem. C* **2018**, *122*, 10956.
[12] R. Ma, G. Lin, Y. Zhou, Q. Liu, T. Zhang, G. Shan, M. Yang, J. Wang, *NPG Comput. Mater.* **2019**, *5*, 78.
[13] H. Zhang, P. An, W. Zhou, B. Y. Guan, P. Zhang, J. Dong, X. W. D. Lou, *Sci. Adv.* **2018**, *4*, eaao6657.
[14] C. R. Rajamathi, U. Gupta, N. Kumar, H. Yang, Y. Sun, V. Suss, C. Shekhar, M. Schmidt, H. Blumtritt, P. Werner, B. Yan, S. Parkin, C. Felser, C. N. R. Rao, *Adv. Mater.* **2017**, *29*, 1606202.
[15] G. Li, C. Fu, W. Shi, L. Jiao, J. Wu, Q. Yang, R. Saha, M. E. Kamminga, A. K. Srivastava, E. Liu, A. N. Yazdani, N. Kumar, J. Zhang, G. R. Blake, X. Liu, M. Fahlman, S. Wirth, G. Auffermann, J. Gooth, S. Parkin, V. Madhavan, X. Feng, Y. Sun, C. Felser, *Angew. Chem., Int. Ed.* **2019**, *58*, 13107.
[16] G. Li, Q. Xu, W. Shi, C. Fu, L. Jiao, M. E. Kamminga, M. Yu, H. Tuysuz, N. Kumar, V. Suss, R. Saha, A. K. Srivastava, S. Wirth, G. Auffermann, J. Gooth, S. Parkin, Y. Sun, E. Liu, C. Felser, *Sci. Adv.* **2019**, *5*, eaaw9867.
[17] H. Chen, W. Zhu, D. Xiao, Z. Zhang, *Phys. Rev. Lett.* **2011**, *107*, 056804.
[18] J. P. Xiao, L. Z. Kou, C. Y. Yam, T. Frauenheim, B. H. Yan, *ACS Catal.* **2015**, *5*, 7063.
[19] L. Li, J. Zeng, W. Qin, P. Cui, Z. Zhang, *Nano Energy* **2019**, *58*, 40.

[20] J. Li, H. Ma, Q. Xie, S. Feng, S. Ullah, R. Li, J. Dong, D. Li, Y. Li, X. Q. Chen, *Sci. China Mater.* **2018**, *61*, 23.
[21] B. Hammer, J. K. Nørskov, *Adv. Catal.* **2000**, *45*, 71.
[22] H. Zhang, C. X. Liu, X. L. Qi, X. Dai, Z. Fang, S. C. Zhang, *Nat. Phys.* **2009**, *5*, 438.
[23] A. Bansil, H. Lin, T. Das, *Rev. Mod. Phys.* **2016**, *88*, 021004.
[24] B. Yan, B. Stadtmuller, N. Haag, S. Jakobs, J. Seidel, D. Jungkenn, S. Mathias, M. Cinchetti, M. Aeschlimann, C. Felser, *Nat. Commun.* **2015**, *6*, 10167.
[25] J. L. Manes, *Phys. Rev. B* **2012**, *85*, 155118.
[26] N. B. Schröter, D. Pei, M. G. Vergniory, Y. Sun, K. Manna, F. de Juan, J. A. Krieger, V. Süss, M. Schmidt, P. Dudin, *Nat. Phys.* **2019**, *15*, 759.
[27] G. Chang, S. Y. Xu, B. J. Wieder, D. S. Sanchez, S. M. Huang, I. Belopolski, T. R. Chang, S. Zhang, A. Bansil, H. Lin, M. Z. Hasan, *Phys. Rev. Lett.* **2017**, *119*, 206401.
[28] G. Chang, B. J. Wieder, F. Schindler, D. S. Sanchez, I. Belopolski, S. M. Huang, B. Singh, D. Wu, T. R. Chang, T. Neupert, S. Y. Xu, H. Lin, M. Z. Hasan, *Nat. Mater.* **2018**, *17*, 978.
[29] P. Tang, Q. Zhou, S. C. Zhang, *Phys. Rev. Lett.* **2017**, *119*, 206402.
[30] B. Bradlyn, J. Cano, Z. Wang, M. G. Vergniory, C. Felser, R. J. Cava, B. A. Bernevig, *Science* **2016**, *353*, aaf5037.
[31] D. J. Rebar, S. M. Birnbaum, J. Singleton, M. Khan, J. Ball, P. Adams, J. Y. Chan, D. Young, D. A. Browne, J. F. DiTusa, *Phys. Rev. B* **2019**, *99*, 094517.
[32] O. Gunnarsson, R. O. Jones, *Phys. Rev. B: Condens. Matter* **1985**, *31*, 7588.
[33] D. C. Langreth, M. J. Mehl, *Phys. Rev. B* **1983**, *28*, 1809.
[34] J. P. Perdew, *Phys. Rev. Lett.* **1985**, *55*, 1665.
[35] D. Rees, K. Manna, B. Lu, T. Morimoto, H. Borrmann, C. Felser, J. Moore, D. H. Torchinsky, J. Orenstein, arXiv:1902.03230 **2019**.
[36] N. Schröter, S. Stolz, K. Manna, F. de Juan, M. G. Vergniory, J. A. Krieger, D. Pei, P. Dudin, T. K. Kim, C. Cacho, arXiv:1907.08723 **2019**.
[37] J. Kibsgaard, T. F. Jaramillo, F. Besenbacher, *Nat. Chem.* **2014**, *6*, 248.
[38] Y. Zheng, Y. Jiao, Y. Zhu, L. H. Li, Y. Han, Y. Chen, M. Jaroniec, S. Z. Qiao, *J. Am. Chem. Soc.* **2016**, *138*, 16174.
[39] J. Mahmood, F. Li, S. M. Jung, M. S. Okyay, I. Ahmad, S. J. Kim, N. Park, H. Y. Jeong, J. B. Baek, *Nat. Nanotechnol.* **2017**, *12*, 441.
[40] Y. Zhu, H. A. Tahini, Z. Hu, J. Dai, Y. Chen, H. Sun, W. Zhou, M. Liu, S. C. Smith, H. Wang, Z. Shao, *Nat. Commun.* **2019**, *10*, 149.
[41] Y. T. Li, F. Q. Chu, Y. Liu, Y. Kong, Y. X. Tao, Y. X. Li, Y. Qin, *Chem. Commun.* **2018**, *54*, 13076.
[42] V. Dusastre, *Materials for Sustainable Energy: A Collection of Peer-Reviewed Research and Review Articles from Nature Publishing Group*, World Scientific, London, UK **2011**.